Journal of Applied Physics ARTICLE scitation.org/journal/jap

In situ measurements of non-equilibrium positron state defects during He irradiation in Si

Cite as: J. Appl. Phys. **133**, 185901 (2023); doi: 10.1063/5.0144308
Submitted: 29 January 2023 · Accepted: 11 April 2023 ·
Published Online: 8 May 2023

R. Auguste,[1] M. O. Liedke,[2] M. Butterling,[2] B. P. Uberuaga,[3] F. A. Selim,[4,5] A. Wagner,[2] and P. Hosemann[1,6,7,a)]

AFFILIATIONS

[1]Department of Nuclear Engineering, University of California at Berkeley, Berkeley, California 94720, USA
[2]Institute of Radiation Physics, Helmholtz-Zentrum Dresden-Rossendorf, Bautzner Landstr. 400, 01328 Dresden, Germany
[3]Materials Science and Technology Division, Los Alamos National Laboratory, Los Alamos, New Mexico 87545, USA
[4]Center for Photochemical Sciences, Bowling Green State University, Bowling Green, Ohio 43403, USA
[5]Department of Physics and Astronomy, Bowling Green State University, Bowling Green, Ohio 43403, USA
[6]Lawrence Berkeley National Laboratory, Material Science Division, Berkeley, California 94720, USA
[7]Department of Mechanical Engineering, University of California at Berkeley, Berkeley, California 94720, USA

[a)]**Author to whom correspondence should be addressed:** peterh@berkeley.edu

ABSTRACT

Radiation-induced property changes in materials originate from the energy transfer from an incoming particle to the existing lattice, displacing atoms. The displaced atoms can cause the formation of extended defects including dislocation loops, voids, or precipitates. The non-equilibrium defects created during damage events determine the extent of these larger defects and are a function of dose rate, material, and temperature. However, these defects are transient and can only be probed indirectly. This work presents direct experimental measurements and evidence of irradiated non-equilibrium vacancy formation, where *in situ* positron annihilation spectroscopy was used to prove the generation of non-equilibrium defects in silicon.

INTRODUCTION

Radiation damage in materials can lead to physical[1,2] and chemical property[3,4] changes in the materials, therefore degrading the properties of components and further limiting its performance and lifetime. In the first instance, the energy transfer from the incoming radiation to the host atoms creates non-equilibrium defects. The evolution of these defects can, depending on conditions, lead to the formation of extended defects and, therefore, property changes and premature failure of the material or component. The buildup of extended defects is governed by how the initial point defects interact with each other and with pre-existing microstructural features such as grain boundaries or dislocations over time. As such, radiation damage is truly multiscale in space and time, from atomic-sized point defects formed in femtoseconds to degradation of entire reactor pressure vessels over decades.[5] The consequences of radiation effects manifest themselves in phenomena such as swelling, hardening, and embrittlement that occur on the macroscopic scale, but the underlying physics is based on time and length scale relevant features within the material that are incredibly difficult to probe directly.[6]

Within the first interaction of radiation with matter, there are a large number of transient displacements in the radiation cascade, but most self-anneal within a time scale on the order of picoseconds,[6,7] leaving just a relatively small number of defects. The conventional rate theory suggests that there is a buildup of a steady-state concentration of defects generated during irradiation as a function of dose rate, pre-existing microstructural feature, and temperature.[8] Mobile Frenkel pairs (vacancies and interstitials) formed throughout the solid during irradiation randomly move until they cease to exist either by recombination with the opposite type of defect or by incorporation into the lattice at fixed sinks such as dislocations, grain boundaries, and voids.[8] While these remaining non-equilibrium defects can be characterized by probes such as x-ray diffraction (XRD) and transmission electron

microscopy (TEM),[9,10] capturing the transient, small point defects that drive their evolution must be done *in situ*, before they anneal out or aggregate into larger, extended, more stable defects.

The small size and non-equilibrium nature of the transient point defects makes a direct observation difficult. Instead, measurement tools have focused on observing larger defects or measure the effects of radiation indirectly by sampling other properties. Differential dilatometry,[11] electrical resistivity measurements,[12] or short, intense ion beam pulses[13] have been used to study the results of displacement cascades and the extended damage. Furthermore, stable defects such as dislocation loops, voids, and cavities larger than 1–2 nm can be observed using TEM studies or various diffraction techniques.[14–16]

Studies observe and quantify these extended effects of radiation damage but do not provide direct insight into the transient defects, which drive the development of those extended effects. The survival of defects is a dynamic problem, so the experimental verification of either the displacement damage or its evolution has proven to be difficult. *In situ* techniques must be employed to experimentally quantify and verify the evolution of the damage cascade.

Positrons are a fundamental particle that can be used as a nondestructive analytical probe to study vacancy-type defects in nearly all material classes.[17] Positron annihilation spectroscopy (PAS) introduces positrons (antiparticles of electrons) to a material, where they thermalize, diffuse, and, eventually, annihilate with the electrons present in matter.[18] The presence of defects in a material alters the interaction of positrons with electrons and changes the resulting 511 keV annihilation gamma radiation signal, which leads to the fact that positrons in matter can act as a probe for vacancy-type defects. PAS can be categorized in two main areas. In the presence of defects, Doppler broadening variable energy positron annihilation spectroscopy (DB-VEPAS) studies the electron momentum distribution around the defect site, while variable energy positron annihilation lifetime spectroscopy (VEPALS) studies the lifetime of the trapped positrons as a function of depth. Positrons have been used for many years to study radiation damage in materials, albeit almost exclusively postmortem.[19]

In DB-VEPAS, the S-parameter, which corresponds to the annihilation fraction with low electron momentum valence electrons, and open-volume defects are correlated, allowing one to observe relative changes in the density of defects. The W-parameter represents the annihilation fraction with high momentum core electrons and can be utilized to reveal the elemental decoration of the annihilation site by performing coincident DB-VEPAS.[20] Previous *in situ* experiments have attempted DB-PAS[21,22] using low energy positrons with low penetration depth into irradiated samples.[23,24] These studies did not implant monoenergetic positrons, leading to limiting depth resolution. In contrast, variable energy positron annihilation spectroscopy (VEPAS) allows for depth-resolved measurements of vacancy-type defects in a material with a continuous or pulsed, monoenergetic positron beam.

While experimental facilities with monoenergetic positron beams are limited, previous studies have demonstrated the usefulness of *ex situ* VEPAS for studying surviving vacancy-type defects in ion-implanted and irradiated materials in materials like silicon.[20]

In the work discussed here, non-equilibrium defects were studied using *in situ* DB-VEPAS during ion irradiation featuring 5 keV He^+ in Si. This study focuses on silicon to exclude any other microstructural features and to investigate whether and how *in situ* DB-VEPAS can be used to characterize the changes as a function of dose in a material.

MATERIALS AND METHODS

The commercially available n-type Si wafer was obtained. Silicon was chosen because its defect dynamics at low doses are well-studied, especially with positrons, mostly due to the prolific use of ion implantation in the semiconductor industry. In addition, silicon wafers provide readily available defect free substrates for investigating contrasts with ion-induced defects and other microstructural effects can be excluded. Furthermore, in rate theory, the defect sinks (dislocations) are an input parameter and higher defect sink concentration can lead to significant different outcomes. Therefore, Si with no defect sinks is an ideal material to proof this approach. In addition, the current setup is limited in its ion beam energy and, therefore, a low-density material like silicon can increase the penetration depth.

DB-VEPAS measurements were performed at the positron facility in the Helmholtz-Zentrum Dresden-Rossendorf (HZDR) in Dresden, Germany. The DB-VEPAS measurements were conducted at the apparatus for *in situ* defect analysis (AIDA)[21] of the slow positron beamline (SPONSOR).[22] Positrons were implanted into each sample with discrete kinetic energies E_p in the range between 0.05 and 10 keV, which allows for depth profiling from the surface down to about 650 nm. Before performing any experiments with the ion beam, a characterization of the bulk Si was done with DB-VEPAS. These results were compared after the beam cycling experiment and subsequent sample exposure to oxidation to characterize overall changes in the sample structure during the experiment.

The positron implantation profile is described by the exponential probability density function, $P(z)$, in the following equation:[25]

$$P(z) = \frac{1}{\langle z \rangle} e^{-\frac{z}{\langle z \rangle}}, \tag{1}$$

where z is the depth from the sample surface. The mean penetration depth of positrons, $\langle z \rangle$, is given by the Makhov positron stopping expression as a function of positron implantation energy, E_p, using the following equation:[25]

$$\langle z \rangle = \frac{A}{\rho} (E_p)^n, \tag{2}$$

where $A = 3.6\ \mu g/cm^2\ keV^{-1.6}$ and $n = 1.6$ are the independent empirical parameters[26] and ρ is the material density, which is considered here to be $2.329\ g/cm^3$ for pure Si. This stopping profile does not consider subsequent diffusion of positrons or formation of positronium. Positronium formation is expected at the surface for shallow ion irradiations and can be characterized using the 3g2g signal representing ortho-positronium (o-Ps) formation. o-Ps

is generated at surfaces of pores and at the film/vacuum interface. Epithermal and thermally excited positrons can reach the surface easier and contribute to the o-Ps emission in defect free crystals.[27] Unfortunately, the formation of positronium makes very shallow experiments difficult to interpret. However, we believe that 2.45 keV mostly probe bulk properties and not surface states since the peak of the implantation depth is slightly more than 50 nm.

For DB-VEPAS data acquisition, thermalized positrons have very small momentum compared to the electrons upon annihilation, and a broadening of the 511 keV line is observed mostly due to momentum of the electrons, which is measured with one or two high-purity Ge detectors (energy resolution of 1.09 ± 0.01 at 511 keV). This broadening is characterized by two distinct parameters S and W defined as a fraction of the annihilation line in the middle (511 ± 0.70 keV) and outer regions (508.56 ± 0.30 and 513.44 ± 0.30 keV), respectively. The S-parameter is a fraction of positrons annihilating with low momentum valence electrons and represents vacancy-type defects and their concentration. The W-parameter approximates the overlap of positron wavefunction with high momentum core electrons.[28,29]

The He^+ ion gun used for room-temperature irradiation was a Kaufman type with defocused beam area of about 5 mm in diameter and an ion current of up to 1 mA. The highest ion implantation energy available was used, 5 keV, in order to drive the ions as deep into the sample as possible as to minimize surface contributions. The positron implantation energy was chosen to be at the maximum of the ion implantation depth. Unfortunately, as of today, no higher energy ion source is available at the positron facility.

To measure the non-equilibrium vacancy defect survival, DB-VEPAS was performed before and during ion irradiation at 30-min intervals at room temperature. This irradiation-measurement iteration pattern was performed three times to allow for the relaxation of non-equilibrium defects. The objective was to observe how the open-volume defects from radiation damage change the S-parameter during and after ion irradiation.

The depth-resolved positron measurements were taken in 30-min intervals at $E_p = 2.45$ keV (about 200 kcnts at 511 keV peak) before (b_i) and during (d_i) irradiation, where i, is the irradiation iteration step. The ion implantation was 5 keV He^+ with $I_{ion} = 100$ nA. After the last irradiation, a DB-VEPAS measurement was taken at $E_p = 2.45$ keV, labeled "after" (a).

Ideally, all implanted positrons would sample defects created by incoming ions, so both the ion and positron implantation profiles were simulated to find a maximum overlap. The ion implantation depth profile was simulated using SRIM Monte Carlo.[30] The beam fluence to damage conversion is based on SRIM Monte Carlo code simulations using the K–P mode with displacement threshold energy to calculate the displacement per atom (dpa) of 40 eV for Si. The Makhov positron implantation profile was simulated for positron energies (E_p) from 2.45 keV in Si. Figure 1 shows the overlapped ion and positron implantation profiles. Maximum overlap between positron implantation and ion damage was calculated at $E_p \approx 3$ keV, so $E_p = 2.45$ keV was chosen for the *in situ* measurements. We found that a slightly lower energy may be more appropriate to choose in order to account for the fact

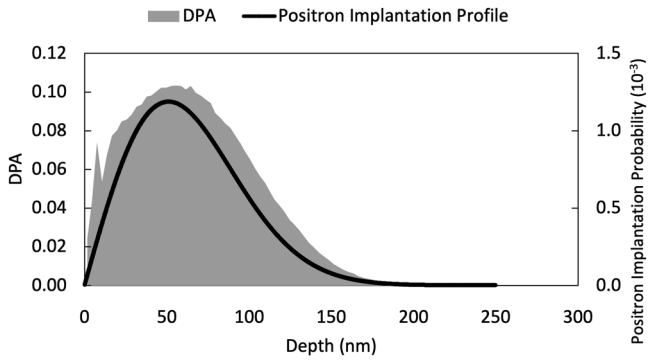

FIG. 1. Ion implantation damage profile calculated from SRIM (shaded in gray) and positron implantation profile at 2.45 keV (black). The He^+ implantation peak is slightly ahead of the displacement per atom (dpa) curve. The maximum overlap between positron implantation and ion damage was found at $E_p = 2.45$ keV, which determined the positron energy for the *in situ* measurements.

that positrons have a diffusion length, and we reduce the amount of non-irradiated material being sampled.

After *in situ* DB-VEPAS, variable energy positron annihilation lifetime spectroscopy (VEPALS) measurements were conducted on two Si samples at the mono-energetic positron source (MePS) beamline at HZDR, Germany:[22,31] one pristine and the post-irradiation Si sample. Positrons were implanted into each sample with discrete kinetic energies E_p in the range between 0.5 and 12 keV, which allows for depth profiling from the surface down to about 850 nm.

The MePS beamline is the end station of the radiation source ELBE (Electron Linac for beams with high Brilliance and low Emittance) at HZDR (Germany),[22,31] featuring a digital lifetime $CrBr_3$ scintillator detector [51 mm diameter (2 in.) and 25.4 mm length (1 in.)] coupled with a Hamamatsu R13089-100 PMT with a μ-metal shield and housed inside a solid Au casing with a homemade software employing a SPDevices ADQ14DC-2X with 14 bit vertical resolution and 2 GS/s horizontal resolution and with a time resolution function down to about 0.230 ns.[32] The resolution function required for spectrum analysis uses two Gaussian functions with distinct intensities depending on the positron implantation energy, E_p, and appropriate relative shifts. All spectra contained at least 1×10^7 counts.

A typical lifetime spectrum N(t) is described by $N(t) = \Sigma\,(1/\tau_i)\, I_i \exp(-t/\tau_i)$, where τ_i and I_i are the positron lifetime and intensity of the ith component, respectively ($\Sigma I_i = 1$). All the spectra were deconvoluted using the non-linearly least-squared based package PALSfit fitting software[33] into few discrete lifetime components, which directly evidence few different defect types (sizes) (see Fig. 4). The corresponding relative intensities reflect to a large extent concentration of each defect type (size). In general, positron lifetime is directly proportional to the defect size, i.e., the larger the open volume, the lower the probability and the longer it takes for positrons to be annihilated with electrons.[34–36] Positron lifetimes and intensities were measured as a function of positron implantation energy, E_p, or mean implantation depth, $\langle z \rangle$.

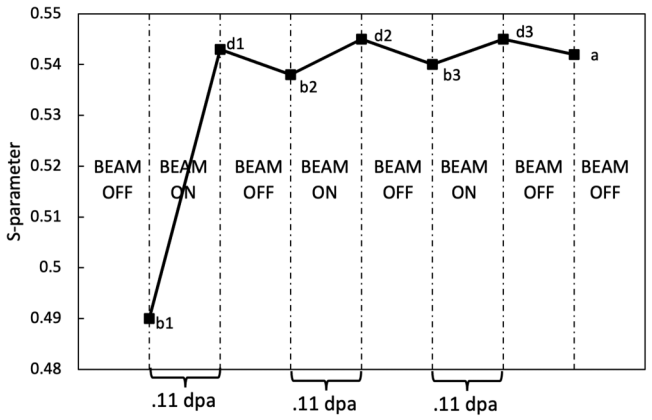

FIG. 2. S-parameters from 30-min DB-VEPAS acquisition at $E_p = 2.45$ keV (about 200 kcnts at 511 keV peak) before (b_i) and during (d_i), where i is the irradiation iteration step. For all irradiation steps, $I_{ion} = 100$ nA. Errors are of the symbol size.

RESULTS AND DISCUSSION

DB-VEPAS measurements were recorded during each irradiation iteration step with the ion beam either on or off. The results are shown in Fig. 2, featuring S-parameters from each 30-min DB-VEPAS acquisition at $E_p = 2.45$ keV (about 200 kcnts at 511 keV peak) before (b_i) and during (d_i) irradiation. The relative increase in the S-parameter during irradiation steps suggests the development of defects. However, the drop after the ion beam is turned off can be induced by either transient or defect states. But again, we believe the changes are due to the defect states and not surface states since the implantation peak is below 50 nm depth. Furthermore, monovacancies have been found to be unstable (mobile) in Si at room temperatures, so the formation of more stable divacancies is likely.[37] The most important finding seen in Fig. 2 is the increased S-parameter values during each irradiation step with the ion beam on (d_i) compared to the measurements before an irradiation step (b_i) with the ion beam off, which most likely probes a small fraction of non-equilibrium vacancies.

In addition to the increase in the S-parameter after each irradiation, the difference in the S-parameter between beam on/off seems to decrease with each iteration step, suggesting the buildup of defects in the irradiated Si.

Despite apparent defect buildup, Si amorphization is not expected in this study because of the low dose delivered during irradiation. Dividing the beam current by the area gives an estimated dose per 30-min irradiation of 9.8×10^{14} ions/cm^2. The total dose delivered to the sample is an order of magnitude less than the experimental threshold for Si amorphization at 8×10^{16} ions/cm^2.[38,39] Amorphization can be limited because of recombination of point defects and surface annihilation from doses with light ions at low energies.[38–40] From SRIM, this incoming dose can be used to calculate overall dpa level. From each 30-min. irradiation, about 0.11 dpa is expected according to the SRIM simulations utilizing aforementioned fluence. Figure 2 shows the S-parameters of each irradiation step as a function of dpa delivered.

The DB-VEPAS measurements at $E_p = 2.45$ keV sampled the peak ion damage from irradiation, but other damaged regions in the sample were assessed after the last irradiation iteration step i = 3. Figure 3(a) shows an increase in the S-parameter after irradiation was seen at each positron energy from 0.5 to 10 keV. At the end of the beam cycling experiment, the vacuum chamber was vented to expose the sample to air at room temperature. The decrease in the S-parameter after the sample is exposed to air is attributed to the formation of an oxide layer on the surface, but the deeper damage still remains. The increased ortho-positronium (o-Ps) fraction after irradiation suggests surface oxide removal, which changes surface defect states and likely is responsible for the abrupt increase in S after the first irradiation step [Fig. 3(b)].[41] The near-surface SiO_2/Si region clearly changes with ion irradiation, even with light ions. TRIM calculations and acoustic impedance measurements[42] predict that this mechanism is due to defect formation and recoil of the native oxide atoms into the near-surface silicon region. Future studies can explore deeper ion implantations in more detail with higher damage profiles away from the surface,

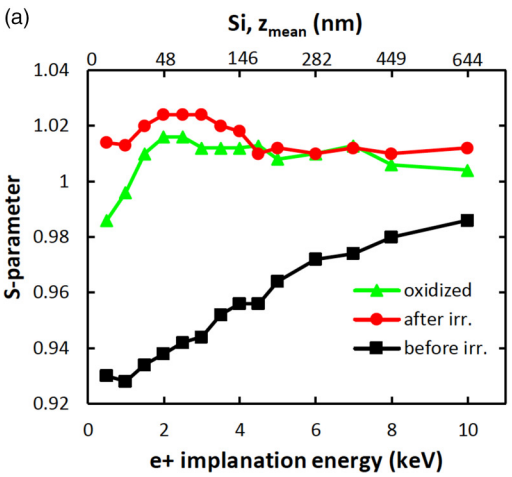

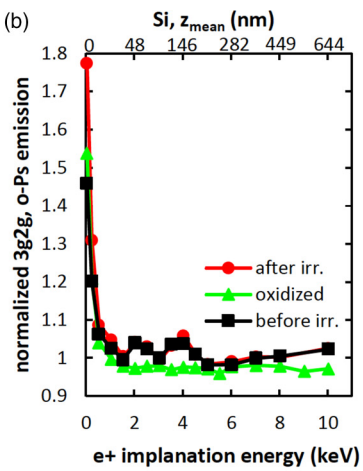

FIG. 3. (a) DB-VEPAS measurements before (black squares) irradiation and after the last irradiation iteration step i = 3 (red circles) and after the sample exposition to air (green triangles). The measurements used a range of positron energies from 0.5 to 10 keV, and the expected depth from the sample surface sampled (z) is shown as well. Figure 3(b) shows the normalized 3g2g emission. Errors are of the symbol size.

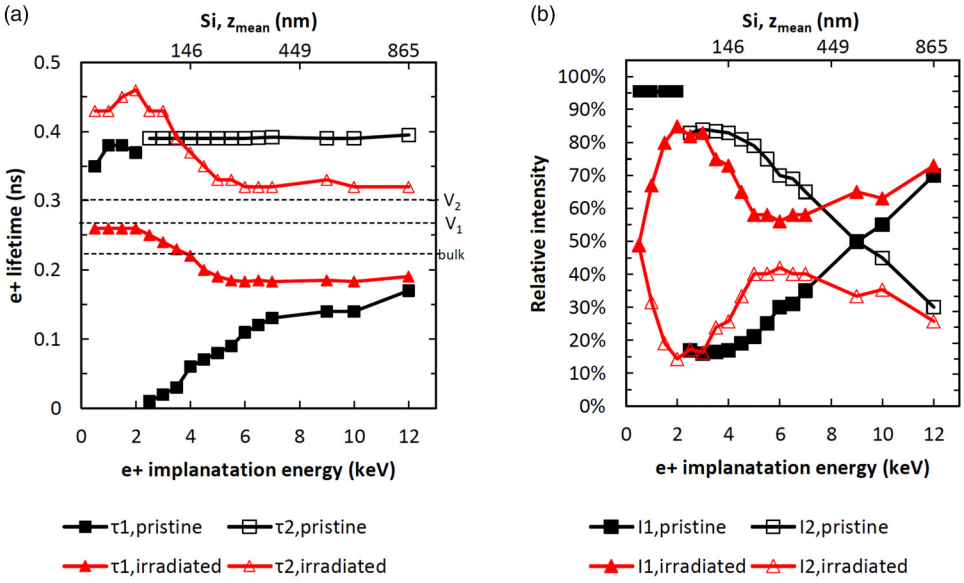

FIG. 4. VEPALS analysis for pristine (closed symbols) and He^+ irradiated (open symbols) Si substrate. (a) The first τ_1 (squares) and the second τ_2 (circles) lifetime components as a function of positron implantation energy and mean positron implantation depth, <z>, and (b) the lifetime components' relative intensities I_1 and I_2, respectively. Errors are of the symbol size.

removing surface effects. A follow-up study could, for example, use heavier implantation ions to create different defect types such as dislocation loops, larger vacancy clusters, and even amorphous irradiated regions in the crystalline substrate.

Considering the existing DFT calculations (local-density approximation scheme with the Boronski and Nieminen enhancement)[43] of defect states in Si, a change in the S-parameter with respect to its bulk value (S_B) corresponding to a monovacancy is $S/S_B \approx 1.018$. For a divacancy, $S/S_B \approx 1.045$ is expected. The final *in situ* S-parameter value after irradiation in the maximum damage region between 50 and 100 nm lies between these two defect states, indicating that the maximum cluster size is a divacancy.

The size of vacancies has been also confirmed by *ex situ* depth-resolved variable energy positron annihilation lifetime spectroscopy (VEPALS) measurements. Figure 4 depicts VEPALS for the pristine and irradiated samples as a function of positron implantation energies. The upper x axis represents the positron mean implantation depth.

Figure 4 shows the first 20–30 nm region of the pristine sample is dominated by large vacancy clusters (>5 vacancies), since only a single lifetime component is detected, $\tau_1 \approx 385$ ps ($I_1 \approx 99\%$). In the deeper parts of the sample, two lifetime components have been detected, where the first component τ_1 is less than the bulk lifetime in Si[44] and, thus, represents the reduced bulk lifetime, and the second component τ_2 represents a defect component. This strongly indicates the defect free existence of the initial state of Si, despite surface effects. The long positron diffusion length in defect free Si allows for a fraction of positrons to reach the surface oxide and annihilate. After irradiation, the first 100 nm is changed completely. The vacancy cluster size increases ($\tau_2 > 400$ ps; vacancy clustering), and a large number of most likely monovacancies (V_1 in Fig. 4) are introduced ($\tau_1 \approx 262$ ps).[45] The profiles of relative intensities resemble the ion damage profile, especially the τ_2 profile. Deeper in the irradiated sample, a signature of divacancies (V_2) or slightly larger defects is found. This divacancy signature found in VEPALS agrees directly with the DB-VEPAS results in which divacancies are also observed as the major defect fraction.

This study is the first of its kind measurement attempting to measure the non-equilibrium defects during irradiation. However, due to experimental limitations today it can only measure relative changes in defect concentration, as opposed to VEPALS, which can quantify absolute changes. Future experiments should investigate the changes in absolute non-equilibrium defect population under irradiation and annealing. *In situ* investigations under extreme environments will promote the understanding of non-equilibrium defect contribution to extended deformation effects of materials under corrosion, pressure, or stress.

Further limitations of this study are the range of ion implantation (the peak range of approximately 50 nm) due to experimental limitations. Shallow ion implantations complicate analysis because of the surface effects that are present within 100 nm, especially the positron implantation distribution superimposed with at least partial back diffusion of positrons to the surface and the surface 2–3 nm oxide that complicates a detailed analysis. In the future, deeper ion implantations must be performed to combat the effect of diffusion and formation of positronium or other surface effects.

SUMMARY

The effect of non-equilibrium defects from radiation damage in Si was investigated by *in situ* depth-resolved DB-VEPAS measurements during ion irradiation. Cycling the ion beam on and off allowed for the investigation of non-equilibrium defect populations during and after irradiation with positron spectroscopy. Significant increases in the defect population were observed as S-parameter values during irradiation (ion beam on) were higher compared to when the ion beam was off, which indicates the presence of non-equilibrium vacancies. The decreases in the S-parameter after

turning the ion beam off highlighted the importance of *in situ* measurements for capturing the relaxation of the non-equilibrium vacancies induced by irradiation. From the absolute S-parameter increase, the defect states were determined to be a mixture of mono- and di-vacancies. Shallow ion implantation and DB-VEPAS measurements limited this study to the relative investigation of defect population, but in the future, *in situ* VEPALS with irradiation could quantify true defect populations of non-equilibrium vacancies. Further *in situ* studies are needed to understand the true defect concentration of materials during irradiation, as that will drive the materials' response in a number of contexts, including irradiation environments with added corrosion, pressure, or stress.

ACKNOWLEDGMENTS

This work was supported as part of FUTURE (Fundamental Understanding of Transport Under Reactor Extremes), an Energy Frontier Research Center funded by the U.S. Department of Energy, Office of Science, Basic Energy Sciences and was supported by the U.S. Department of Energy through the Los Alamos National Laboratory. Los Alamos National Laboratory is operated by Triad National Security, LLC, for the National Nuclear Security Administration of U.S. Department of Energy (Contract No. 89233218CNA000001). Parts of this research were carried out at ELBE at the Helmholtz-Zentrum Dresden-Rossendorf (HZDR), a member of the Helmholtz Association. We would like to thank the facility staff (Ahmed G. Attallah and Eric Hirschmann) for their assistance. This work was partially supported by the Impulse-und Net-working fund of the Helmholtz Association (No. FKZ VH-VI-442 Memriox) and the Helmholtz Energy Materials Characterization Platform (No. 03ET7015) and was also supported by the Ron & Gail Gester Fellowship at the University of California, Berkeley.

AUTHOR DECLARATIONS

Conflict of Interest

The authors have no conflicts to disclose.

Author Contributions

R. Auguste: Data curation (equal); Investigation (equal); Writing – original draft (equal). **M. O. Liedke:** Investigation (equal); Writing – original draft (equal); Writing – review & editing (equal). **M. Butterling:** Methodology (equal); Writing – review & editing (equal). **B. P. Uberuaga:** Funding acquisition (equal); Supervision (equal); Writing – review & editing (equal). **F. A. Selim:** Conceptualization (equal); Investigation (equal); Supervision (equal). **A. Wagner:** Project administration (equal); Writing – review & editing (equal). **P. Hosemann:** Conceptualization (equal); Funding acquisition (equal); Investigation (equal); Supervision (equal); Writing – review & editing (equal).

DATA AVAILABILITY

The data that support the findings of this study are available from the corresponding author upon reasonable request.

REFERENCES

[1]F. Schmidt, P. Hosemann, R. O. Scarlat, D. K. Schreiber, J. R. Scully, and B. P. Uberuaga, Ann. Rev. Mater. **51**, 293–328 (2021).
[2]A. P. C. Wyliem, K. B. Woller, S. A. A. Al Dajani, B. R. Dacus, E. J. Pickering, M. Preuss, and M. P. Short, J. Appl. Phys. **132**, 045102 (2022).
[3]H. Kim, M. R. Chancey, T. Chung, I. Brackenbury, M. O. Liedke, M. Butterling[3], E. Hirschmann, A. Wagner, J. K. Baldwin, B. K. Derby, N. Li, K. H. Yano, D. J. Edwards, Y. Wang, and F. A. Selim, Appl. Phys. **132**, 105901 (2022).
[4]M. Hong, A. L. Morales, H. L. Chan, D. D. Macdonald, M. Balooch, Y. Xie, E. Romanovskaia, J. R. Scully, D. Kaoumi, and P. Hosemann, Appl. Phys. **132**, 185104 (2022).
[5]D. J. Bacon and Y. N. Osetsky, Mater. Sci. Eng.: A **365**, 46–56 (2004).
[6]B. D. Wirth, M. J. Caturla, T. D. De La Rubia, T. Khraishi, and H. Zbib, Nucl. Instrum. Methods Phys. Res., Sect. B **180**(1–4), 23–31 (2001).
[7]J. S. Robach, I. M. Robertson, B. D. Wirth, and A. Arsenlis, Philos. Mag. **83**(8), 955–967 (2003).
[8]H. Wiedersich, Radiat. Effects **12**(1-2), 111–125 (1972).
[9]R. E. Stoller, *Primary Radiation Damage Formation*, 1st ed. (Elsevier Ltd, Amsterdam, 2019), Chap. 1.
[10]M. L. Jenkins, J. Nucl. Mater. **216**, 124–156 (1994).
[11]R. Kerl, J. Wolff, and T. Hehenkamp, Intermetallics **7**, 301–308 (1999).
[12]C. Dimitrov, M. Tenti, and O. Dimitrov, J. Phys. F: Met. Phys. **11**(4), 753–765 (1981).
[13]A. Persaud, J. J. Barnard, H. Guo, P. Hosemann, S. Lidia, A. M. Minor, P. A. Seidl, and T. Schenkel, Phys. Proc. **66**, 604–609 (2015).
[14]D. J. Sprouster, C. Sun, Y. Zhang, S. N. Chodankar, J. Gan, and L. E. Ecker, Sci. Rep. **9**(1), 1 (2019).
[15]A. Lupinacci, K. Chen, Y. Li, M. Kunz, Z. Jiao, G. S. Was, M. D. Abad, A. M. Minor, and P. Hosemann, J. Nucl. Mater. **458**, 70–76 (2015).
[16]Q. Yan, J. Gigax, D. Chen, F. A. Garner, and L. Shao, J. Nucl. Mater. **480**, 420–428 (2016).
[17]R. W. Siegel, Ann. Rev. Mater Sci. **10**, 393–425 (1980).
[18]P. Hautojärvi, *Positrons in Solids*, 1st ed. (Springer-Verlag, Berlin, 1979), pp. 491–522.
[19]F. A. Selim, Mater. Charact. **174**, 110952 (2021).
[20]M. Clement, J. M. M. De Nijs, P. Balk, H. Schut, and A. Van Veen, J. Appl. Phys. **79**, 9029–9036 (1996).
[21]M. O. Liedke, W. Anwand, R. Bali, S. Cornelius, M. Butterling, T. T. Trinh, A. Wagner, S. Salamon, D. Walecki, A. Smekhova, and H. Wende, J. Appl. Phys. **117**(16), 163908 (2015).
[22]A. Wagner, M. Butterling, M. O. Liedke, K. Potzger, and R. Krause-Rehberg, "Positron annihilation lifetime and Doppler broadening spectroscopy at the ELBE facility," AIP Conf. Proc. **1970**, 040003 (2018).
[23]A. Kinomura, R. Suzuki, T. Ohdaira, N. Oshima, B. E. O'Rourke, and T. Nishijima, Phys. Proc. **35**, 111–116 (2012).
[24]A. Kinomura, R. Suzuki, T. Ohdaira, N. Oshima, B. E. O'Rourke, and T. Nishijima, J. Phys.: Conf. Ser. **443**(1), 012043 (2013).
[25]M. J. Puska and R. M. Nieminen, "Theory of positrons in solids and on solid surfaces," Rev. Mod. Phys. **66**(3), 841–897 (1994).
[26]P. Asoka-Kumar and K. G. Lynn, Appl. Phys. Lett. **57**, 1634–1636 (1990).
[27]P. J. Schultz and K. G. Lynn, Rev. Mod. Phys. **60**(3), 701–779 (1988).
[28]A. P. Knights, F. Malik, and P. G. Coleman, Appl. Phys. Lett. **75**(4), 466–468 (1999).
[29]W. Anwand, G. Brauer, M. Butterling, H. R. Kissener, and A. Wagner, Defect Diffusion Forum **331**, 25–40 (2012).
[30]J. F. Ziegler, M. D. Ziegler, and J. P. Biersack, Nucl. Instrum. Methods Phys. Res., Sect. B **268**(11–12), 1818–1823 (2010).
[31]A. Wagner, W. Anwand, A. G. Attallah, G. Dornberg, M. Elsayed, D. Enke, A. E. M. Hussein, R. Krause-Rehberg, M. O. Liedke, K. Potzger, and T. T. Trinh, J. Phys.: Conf. Ser. **791**(1), 012004 (2017).

[32]E. Hirschmann, M. Butterling, U. H. Acosta, M. O. Liedke, A. G. Attallah, P. Petring, M. Görler, R. Krause-Rehberg, and A. Wagner, J. Instrum. **16**(8), P08001 (2021).
[33]J. V. Olsen, P. Kirkegaard, N. J. Pedersen, and M. Eldrup, Phys. Status Solidi C **4**(10), 4004–4006 (2007).
[34]R. Krause-Rehberg and H. S. Leipner, *Positron Annihilation in Semiconductors: Defect Studies* (Springer, Berlin, 1999), p. 378.
[35]F. Tuomisto and I. Makkonen, Rev. Mod. Phys. **85**(4), 1583–1631 (2013).
[36]S. Agarwal, M. O. Liedke A. C. L. Jones, E. Reed, A. A. Kohnert, B. P. Uberuaga, Y. Q. Wang, J. Cooper, D. Kaoumi, N. Li, R. Auguste, P. Hosemann, L. Capolungo, D. J. Edwards, M. Butterling, E. Hirschmann, A. Wagner, and F. A. Selim, Sci. Adv. **6**(31), eaba8437 (2020).
[37]T. E. M. Staab, A. Sieck, M. Haugk, M. J. Puska, T. Frauenheim, and H. S. Leipner, Phys. Rev. B **65**(11), 115210 (2002).
[38]F. F. Morehead, B. L. Crowder, and R. S. Title, J. Appl. Phys. **43**(3), 1112–1118 (1972).
[39]L. Pelaz, L. A. Marqués, and J. Barbolla, J. Appl. Phys. **96**(11), 5947–5976 (2004).
[40]X. Huang, M. Balooch, T. Xie, S. Leuber, and P. Hosemann, J. Appl. Phys. **132**, 025106 (2022).
[41]P. G. Coleman, N. B. Chilton, and J. A. Baker, J. Phys.: Condens. Matter **2**(47), 9355–9361 (1990).
[42]C. S. Gorham, K. Hattar, R. Cheaito, J. C. Duda, J. T. Gaskins, T. E. Beechem, J. F. Ihlefeld, L. B. Biedermann, E. S. Piekos, D. L. Medlin, and P. E. Hopkins, Phys. Rev. B **90**(2), 024301 (2014).
[43]M. Hakala, M. J. Puska, and R. M. Nieminen, Phys. Rev. B **57**, 7621–7627 (1998).
[44]S. Mäkinen, H. Rajainmäki, and S. Linderoth, Phys. Rev. B **42**(17), 11166–11173 (1990).
[45]J. C. M. Robles, E. Ogando, and F. Plazaola, J. Phys.: Condens. Matter **19**(17), 176222 (2007).